INSTITUTE OF PHYSICS PUBLISHING JOURNAL OF PHYSICS: CONDENSED MATTER

J. Phys.: Condens. Matter **18** (2006) 5793–5805 doi:10.1088/0953-8984/18/26/001

Apparent diameter of carbon nanotubes in scanning tunnelling microscopy measurements

L Tapasztó[1], G I Márk[1], A A Koós[1], P Lambin[2] and L P Biró[1]

[1] Research Institute for Technical Physics and Materials Science, H-1525 Budapest, PO Box 49, Hungary
[2] Departement de Physique, FUNDP, 61 Rue de Bruxelles, B-5000 Namur, Belgium

E-mail: tapaszto@mfa.kfki.hu

Received 13 March 2006
Published 16 June 2006
Online at stacks.iop.org/JPhysCM/18/5793

Abstract

Geometric effects influencing scanning tunnelling microscopy (STM) image formation of single wall carbon nanotubes (SWCNTs) were studied within the framework of a simple model potential. We focused on the geometrical effects which may influence the tunnelling probabilities and lead to discrepancies between the apparent height of the nanotubes measured by STM and their real geometrical diameter. We found that there are two main factors responsible for the underestimation of nanotubes diameter by measuring their height in STM images: (1) the curvature of the nanotube affects the cross sectional shape of the tunnelling channel; (2) the decay rate of tunnelling probabilities inside the tunnel gap increases with increasing curvature of the electrodes. For a nanotube with 1 nm diameter an apparent flattening of about 10%, due to these geometry-related effects, is predicted. Furthermore these effects are found to be dependent on the diameter of the tubes and tip–sample distances: an increasing flattening of the tubes is predicted for decreasing tube diameter and increasing tip–sample distance.

(Some figures in this article are in colour only in the electronic version)

1. Introduction

Due to their extraordinary electronic and mechanical properties [1] carbon nanotubes (CNTs) have been in the focus of attention for more than a decade. Several potential applications of CNTs, utilizing their unique properties have already been demonstrated, including CNT transistors [2] and logical circuits [3]. The electronic structure of a freestanding single wall carbon nanotube (SWNT) is uniquely determined by its atomic structure and geometry [4]. These all-carbon molecules can be metallic or semiconducting according to the (n, m) wrapping indices of the graphene sheet. Simple tight-binding theory reproduces this relation remarkably

correctly [5], as verified by *ab initio* calculations [6, 7]. Although these theoretical predictions were made soon after the discovery of the nanotubes, the experimental verification became possible only six years later, when atomically resolved scanning tunnelling microscopy (STM) images and reliable scanning tunnelling spectroscopy (STS) measurements could be achieved on individual SWCNTs [8, 9]. Even today, scanning tunnelling microscopy is the only method that enables us to investigate at the same time both the topology and electronic structure of nanometre-sized objects [10].

Together with theoretical techniques for modelling the electronic structure of surfaces, STM measurements have been successfully applied in real space investigation of various surfaces [11]. However, the STM investigation of carbon nanotubes significantly differs from that of bulk surfaces: (1) the tube has a curvature on a nanometric scale which introduces some important geometrical effects (e.g. the well-known tip convolution effects) in the imaging process [12]; (2) for an STM investigation CNTs have to be deposited on the surface of a conducting support, that gives rise to a second tunnelling gap between the tube and the substrate, besides the STM tip–sample tunnel junction present in all STM measurements.

Theoretical modelling of STM images of CNTs focuses on atomic resolution images, and sophisticated calculations are invoked in order to quantitatively reproduce the contrast observed in experimental images [7, 13]. It was possible to relate the experimentally observed images with the nanotubes' helicity (chiral angle) [7, 13]. However, the real diameter of the tubes, which is also of crucial importance in the identification of the nanotube structure—cannot be inferred in a straightforward way. From experimental findings it is obvious that neither the width nor the height of the CNTs observed in STM measurements is a reliable quantity for determining the precise diameter of the imaged nanotube [12, 14]. For a typical nanotube of 1 nm diameter, the apparent broadening of the tube can reach 300% of the geometric diameter, due to tip convolution effects [12]. Theoretically we can obtain the geometrical diameter by deconvolution [9]; however, this would require the precise knowledge of the specific STM tip geometry, which is not available in the majority of cases.

A more accurate method seems to be measuring the height of the tube which is not affected by convolution effects. However, comparison with STS data [14] and observation of nanotubes with anomalously small apparent heights [15, 16] have led to the conclusion that the apparent height of nanotubes measured by STM may significantly differ from their real diameter. These discrepancies were usually attributed to the following factors: (1) the difference in the electronic structure of the tube and support [8, 12], (2) the presence of the second tunnel junction [12], and (3) the mechanical deformation of the nanotubes due to interaction with the support and STM tip [14]. *Ab initio* calculations show that the deviation in diameter due to the difference in the electronic structure of the (gold) support and the nanotube is smaller than 1% [7, 14].

A more substantial deviation may arise from the mechanical deformation of nanotubes. However, deformation due to van der Waals interaction with the substrate for a nanotube of 1.4 nm diameter gives rise to a deformation of about 2%, which further decreases with decreasing tube diameter [17]. Compression of the nanotube by the STM tip during the measurements may occur; however, significantly decreased apparent heights (as compared to spectroscopic data) were observed for tip–tube distances estimated at 0.4 nm, which is unlikely to result in a compressed tube [14].

In the present paper we propose that the discrepancies between the geometrical diameter and those observed in STM measurements, by measuring the height of the nanotubes relative to the substrate, are due to geometrical and quantum mechanical effects arising from the complex shape of the 3D potential barrier of the STM tip–CNT tunnel junction. We invoke the Bardeen formalism in our description of the tunnelling, and a simple jellium potential

model which allow us to perform analytical calculations. Although the use of a jellium potential might seem oversimplified, in so far as we are dealing with geometrical effects it can be adequately justified. Following the conclusion of Hofer *et al* [18] and Briggs *et al* [11], when modelling atomic resolution STM images, the electronic states of the tip and the surface must be precisely simulated, because these states determine the obtainable contrast, which should be in quantitative accordance with measurements. For this reason in these simulations one has generally to rely on sophisticated methods invoking first principles density functional theory [18–20]. However, in the present work we focus on the height of the nanotube on an HOPG (highly oriented pyrolytic graphite) support (corresponding to a feature size of about 1 nm), rather than imaging the atomic structure of nanotubes with high resolution. In this case one has to bear in mind that STM maps the electronic states of the surface several ångströms outside the surface, where the wavefunctions decay very quickly (approximately a factor of 10 decrease in probability density for every ångström of distance). It therefore requires quite strong electronic effects to overcome relatively small geometrical ones [11]. Because the decay of wavefunctions outside the sample is well reproduced by our model, and modulations of high spatial frequency decay more rapidly with the distance within the tunnel gap [21], we conclude that we can apply our model in order to investigate geometric effects, and the results will be relevant for experiments because of the strong influence of geometry on the phenomena.

Jellium models combined with analytic approximations as well as self-consistent electronic-structure models are widely used in studying the transport properties of various metallic nanowires, where the geometry of the system is playing the major role [22–24]. Experimentally observed confinement effects in finite-size carbon nanotubes can also be reproduced by a simple particle in a box model which can be regarded as a simplified jellium model [7, 25, 26]. In a series of papers we successfully used the combination of wavepacket dynamic methods with a jellium potential to get insight in the tunnelling processes through supported carbon nanotubes, and we were able to cross-correlate experimental and theoretical results as concerning tip convolution effects [27], point contact operating mode [28] or axial charge spreading in nanotubes during the tunnelling [29].

The paper is organized as follows. In section 2, some preliminary results are presented: first the eigenstates of the freestanding jellium CNT are calculated analytically, then the influence of the substrate and STM tip on the energies and wavefunctions of the freestanding nanotube are calculated in order to justify the applicability of the perturbational (Bardeen [30] or transfer Hamiltonian) treatment of tunnelling. In section 3 the tunnelling probabilities through the 'STM tip–CNT', 'CNT–substrate' and 'STM tip–substrate' tunnel junctions are calculated, using the Bardeen formalism. The results are applied in interpreting the decreased apparent height observed in STM measurements of the nanotubes.

Hartree atomic units are used in all formulae except where explicit units are given. International system units are used, however, in all figures and numerical data.

2. Analytically calculated stationary energies and wavefunctions for the jellium model of the carbon nanotubes and proximity effects

In most electronic structure calculations, a basis set of wavefunctions is chosen and the problem is transformed to the one of diagonalizing the Hamiltonian matrix. These methods are well adapted to problems of total energy and band-structure calculations, but are less appropriate for correct calculation of STM images. In tunnelling current calculations, the principal role is played by the tail of the wavefunction at relatively large distances from the sample. The accurate details of these 'tails' contribute little to the total energy, thus most methods treat them rather inaccurately. The only method which permits an accurate calculation of wavefunctions

outside the sample at realistic distances is the explicit integration of the Schrödinger equation, as pointed out by Tersoff [31].

In the transfer Hamiltonian formalism [30] one computes the tunnel current in terms of the wavefunctions determined separately for each electrode in the absence of the others. This method is appropriate when the separation between the electrodes is large, and hence the overlap of the wavefunctions of the two electrodes is small. As a first step we consider the different electrodes separately; further on we will investigate the effects of their interaction using the perturbation theory.

In order to calculate the analytical wavefunctions of a CNT, we solved the stationary Schrödinger equation for the one-electron potential modelling a carbon nanotube with geometrical and material parameters chosen to be consistent with our former wavepacket dynamical (WPD) simulations [27–29]. The CNT is modelled by a cylinder of radius $r_{\text{tube}} = 0.5$ nm with effective surfaces lying $j = 0.071$ nm outside the geometrical surface in order to account for the decrease of the tunnel barrier due to the image potential [27, 32]. A jellium potential of $V(r) = V_0 = -9.81$ eV between the inner and outer effective surfaces models the binding of the electrons in the tube and $V(r) = 0$ in the vacuum gap between the electrodes. In the case of the freestanding nanotube, from symmetry considerations, it was feasible to write the Schrödinger equation in cylindrical coordinates, because the jellium potential of an infinite CNT depends only on the radial coordinate r:

$$V(r,\varphi,z) = V(r) = \frac{1}{2}\frac{m^2 - 1/4}{r^2} + \begin{cases} -9.81\ \text{eV} & r \in \left[r_{\text{tube}} - j, r_{\text{tube}} + j\right] \\ 0 & \text{otherwise} \end{cases} \tag{1}$$

where m is the azimuthal quantum number (see below).

Because of translational symmetry along the axis of the jellium CNT, the axial component of the wavefunction is a plane wave for infinite tube length:

$$\psi(r,\varphi,z) = \psi_{2\text{D}}(r,\varphi)\mathrm{e}^{\mathrm{i}k_z z}. \tag{2}$$

Thus the energy of the axial motion can be separated from the total energy:

$$E(m,k_z) = E_{2\text{D}}(m) + E_{\text{axial}}(k_z) \tag{3}$$

where $E_{2\text{D}}$ is the cross sectional component of the energy, i.e. that corresponding to the $\psi_{2\text{D}}(r,\varphi)$ wavefunction component. For the case of the freestanding infinite CNT and also for the investigation of CNT–support interaction it is enough to consider only the cross sectional component of the wavefunction and the energy, i.e. $\psi_{2\text{D}}(r,\varphi)$ and $E_{2\text{D}}$, because the presence of substrate conserves the translational symmetry of the system along the axis of the tube.

Solving the Schrödinger equation for the real cylindrical geometry eliminates the widely used zone folding approximation [4]. Deviations from zone folding results are of particular importance in the case of small diameter tubes [33, 34]. In our model the radial solution can be written as

$$R_{n,m}(r,E_m) = a_m I_m(r,E_m) + b_m J_m(r,E_m) + c_m Y_m(r,E_m) + d_m K_m(r,E_m), \tag{4}$$

a combination of first and second kind Bessel and modified Bessel functions [35], where n is the radial and m the azimuthal quantum number. The $R_{n,m}(r)$ function determines the decay of the wavefunctions. For our range of parameters there is only one radial solution for each m, hence we omit the radial quantum number in notations. The azimuthal solution is quantized due to the periodic boundary condition in 2π and is doubly degenerate for $m > 0$:

$$\psi_{2\text{D}}(r,\varphi) = R_m(r)\left[C_m \cos m\varphi + S_m \sin m\varphi\right]. \tag{5}$$

Figure 1 shows the ground state and the first two excited states of the freestanding jellium tube. The ground-state is non degenerate, while all excited states are doubly degenerate. By

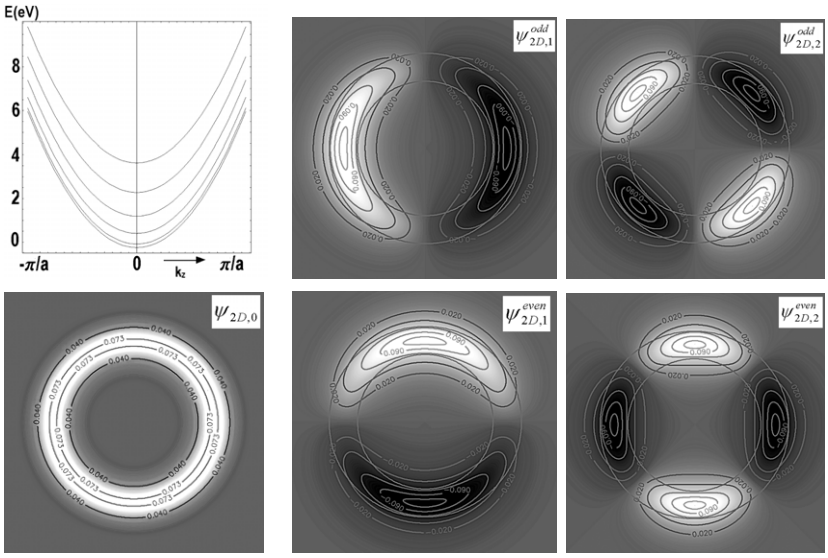

Figure 1. Grey scale cross sectional view of stationary wavefunctions of a jellium tube for different angular momentum quantum eigenstates $m = 0, 1, 2$ respectively. The $m = 0$ ground state is non-degenerate; all the excited states are doubly degenerate. Black corresponds to negative and white to positive wavefunction values. The upper left subfigure shows the one-dimensional band structure of the jellium tube for $m = 0, 1, \ldots 5$. Energy is measured from E_F.

choosing the orthonormal states $\cos m\varphi$ and $\sin m\varphi$ one of the states is an even, and the other an odd function of φ (where the $\varphi = 0$ direction points 'up' towards the tip apex). The one-dimensional band structure of the jellium CNT is shown in the upper left subfigure of figure 1. All bands are parabolic in this model, i.e. the band structure is similar to that of a doped semiconductor CNT.

The similarities between the states of the jellium tube shown in figure 1 and the wavefunctions obtained from *ab initio* calculations based on density functional theory—especially at larger distances from the wall, the region of interest for tunnelling—also confirm the applicability of our model [36, 37]. For example, the squared wavefunction of the state lying 0.5 eV away from the Fermi level of the (8, 0) tube in [36] has a clear fourfold rotational symmetry along the circumference, in good agreement with our results for the $m = 2$ state of the jellium tube.

If one computes the tunnelling current in the perturbational approach, using the electronic states of the freestanding tube, calculated above, it means that the tunnelling states are calculated in the absence of tunnelling, i.e. the wavefunctions are not perturbed by the presence of the additional electrodes: the support, and the STM tip. This approximation can be justified only when the interaction (coupling) of the electrodes is weak, i.e. the wavefunctions of different electrodes overlap only marginally. In order to clarify the applicability of the Bardeen formalism within our potential model, we have investigated the effects of the nearby electrodes (support and STM tip) to the stationary energies and wavefunctions of the freestanding tube.

2.1. The effect of the substrate

CNTs have to be deposited on a conducting substrate for their STM investigation. Metals (Au, Pt) and HOPG (graphite) are used most frequently in experiments. In the case of metal

surfaces the most important effect of the substrate on the STM image is the doping of the CNT [8, 38]. However, this effect is not present when the work functions of the nanotube and substrate are similar, i.e. nanotubes on an HOPG substrate [39]. Another effect is that the proximity of the support perturbs the electronic states of the CNT even when no doping occurs. In order to investigate this effect we choose the same work function and Fermi energy values for our jellium potential model of the CNT and support, in accordance also with the WPD calculations [29], $E_F = 5$ eV, $W = 4.81$ eV. The support surface is modelled by a semi-infinite 3D jellium potential. The nanotube is taken to float 0.335 nm above the support, due to the van der Waals interaction [17].

In order to calculate the first-order perturbation correction, due to the presence of the support, for the non-degenerate $m = 0$ angular momentum quantum state of the nanotube, we have to calculate the integral of the probability density of the unperturbed wavefunction calculated in section 2 over the region where the potential of the support is different from zero:

$$\Delta E_{2D,0} = V_0 \int_{-\infty}^{+\infty} dx \int_{-\infty}^{y_{sup}} dy\, \rho_{2D,0}(x, y) \tag{6}$$

where y_{sup} is the y coordinate of the effective jellium surface of the support (the y axis is perpendicular to the support). The integral gives the probability of finding the quasiparticle in the support region, i.e. $\Delta E_{2D,0} = V_0 p_{sup}$. For the case of an SWNT with 1 nm diameter floating over the substrate at 0.335 nm distance, the energy corresponding to the $m = 0$ angular momentum eigenstate is shifted down by an amount $\Delta E_{2D,0} = -1.48$ meV, which is quite small.

As discussed in section 2, the angular momentum states with nonzero quantum number m are doubly degenerate; hence, in order to calculate the corrections induced by the substrate we have to apply the perturbation theory of degenerate states. The effect of the support for the $m \neq 0$ states is to split the degeneracy. For the case of the $m = 1$ state the energy corrections are $\Delta E^{even}_{2D,1} = -2.89$ meV and $\Delta E^{odd}_{2D,1} = -0.15$ meV. Both of the degenerate states are downshifted, but the energy shift for the odd state is much less than that of the even state because the odd state has a much lower probability density in the support region (figure 1). The splitting of the energies of the nonzero angular momentum quantum states corresponds to the splitting of van Hove singularities in the STS spectra.

Generally, the energy correction due to the presence of the substrate is of order of meV, which shows that the substrate does not seriously affect the electronic structure of the tube. However, this interaction is expected to be strongly dependent on the CNT–support distance; hence we also calculated the dependence of the perturbation energy correction as a function of the tube–substrate distance. An exponential-like dependence was found as shown in figure 2 for the $m = 0$ angular momentum state. Large function values for distances smaller than 0.2 nm indicate the breakdown of perturbation theory for this region. Decreased distances may occur in experiments [28], when a pressure is exerted by the STM tip on top of the CNT.

As concerns the wavefunction of the CNT, its first-order perturbation correction due to the proximity of the support surface is

$$\Delta\psi_{2D,0} = -0.011\psi^{even}_{2D,1} + 0.003\psi^{even}_{2D,2} + \cdots \tag{7}$$

for $s = 0.335$ nm. Only the even states contribute to the wavefunction correction because of the mirror symmetry of the potential. $\Delta\psi_{2D,0}(x, y)$ is shown in figure 3 in the cross section of the CNT. The cylindrical symmetry of the $m = 0$ state is broken; the maximum probability is along the lowest generator of the tube (i.e. that closest to the support).

However, as can be seen from equation (7) and figure 3, the relative amplitude of wavefunction correction is of about 1% of the unperturbed wavefunctions.

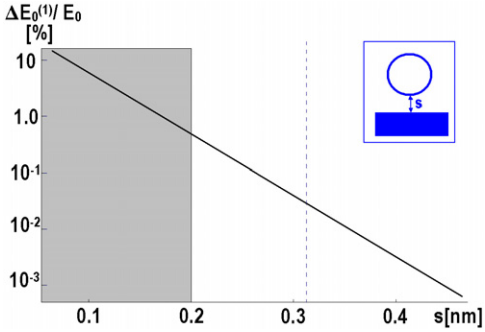

Figure 2. The first-order energy correction (expressed as a percentage of the ground state energy) shows an exponential dependence as a function of CNT–support distance. The shaded region indicates the range where the applicability of the perturbation treatment breaks down. The dashed line indicates the 0.335 nm van der Waals distance.

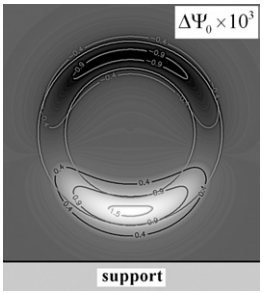

Figure 3. First-order perturbation correction to the ground state wavefunction of the tube due to the proximity of the support surface for 0.335 nm CNT–support distance.

2.2. The effect of the STM tip

The influence of the STM tip, through mechanical tip–sample interactions or multiple tip effects [40], on the STM images has been studied both experimentally and theoretically [41, 42]. When the tip is not in mechanical contact with the sample, it is still possible to affect the sample through the perturbation caused by the tip on the electronic structure of the sample. Tekman and Ciraci identified [43] three ranges for the tip–sample distance in their theoretical examination of the graphene sheet sample–single carbon atom tip model. They pointed out that the tip interacting with the sample induces localized states on the sample surface. For distances smaller than 0.35 nm these so-called tip-induced localized states (TILSs) become pronounced and lead to a modification of the tunnel current.

To study the effect of the tip on the jellium wavefunctions of the CNT we calculated the first-order perturbation correction for the $\psi_{2D,0}$ ground state. Because the tip potential is not translation symmetric along the axis of the CNT (z direction), the perturbation correction contains a weighted sum of all $e^{ik_z z}$ plane waves:

$$\Delta\psi_{2D,0}(r,\varphi,z) = \sum_m \int dz c_m(z)\,\psi_{2D,m}(r,\varphi)\,e^{ik_z z} \tag{8}$$

where $c_m(z)$ is the expansion coefficient obtained from the first-order perturbation expression. As shown in figure 4, $\Delta\psi_{2D,0}$ is a localized state on the CNT surface under the tip apex with a $\Delta z = 1.1$ nm width. To first order the shape of the localized state does not depend on the

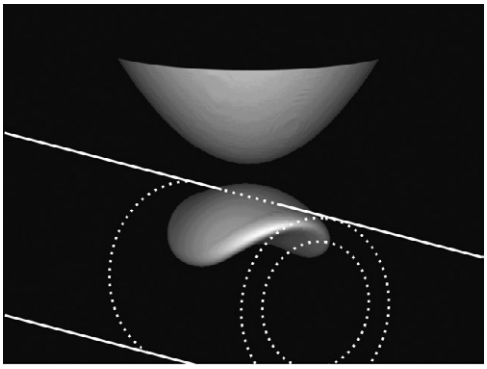

Figure 4. Tip-induced localized state (TILS) on the nanotube visualized by an isodensity surface. White lines show the effective jellium surfaces of the 1 nm diameter nanotube. The axial distance between the broken circles is 1.92 nm. The effective jellium surface of the hyperbolic tip is shown above the tube. The tip–tube distance is 0.409 nm.

tip–sample distance: only its magnitude is increasing exponentially with decreasing distance. For the 0.409 nm tip–CNT distance (consistent with WPD simulations) the relative magnitude of the wavefunction correction (as compared with the unperturbed ground state of the CNT) is only 7×10^{-5}, but for a 0.2 nm separation it already increases to 10^{-2}. This shows that for a 0.409 nm tunnel gap the electronic structure of the CNT is not perturbed significantly by the tip but for a gap smaller than 0.2 nm the TILS [43] has to be taken into account in the tunnel current calculation.

Therefore we conclude that the proximity of the substrate and tip electrodes, which is unavoidable in STM measurements of carbon nanotubes, in typical measurement conditions, does not affect the electronic states of the nanotubes in a decisive way; hence the applicability of perturbational treatment to study tunnelling phenomena within our model can be justified. The above results are confirmed by the small transmission coefficients of about 10^{-3} obtained in WPD simulations—indicating a weak coupling between the electrodes—performed on the same potential model, and are also in accordance with *ab initio* calculations performed on more realistic potential models, but with similar geometries [7].

3. STM currents and tunnelling matrix elements of the tip–tube–support system

In calculating tunnelling currents flowing trough our model system it is desirable to take advantage of the fact that the results of section 2 indicate a weak coupling between the electrodes. In this limit the tunnel current can be written as

$$I = 2\pi \sum_{\mathrm{t,s}} |M_{\mathrm{ts}}|^2 \delta\left(E_{\mathrm{t}} - E_{\mathrm{F}}\right) \delta\left(E_{\mathrm{s}} - E_{\mathrm{F}}\right) \tag{9}$$

where the indices t and s mean the tip and sample, respectively. Nevertheless it is sometimes necessary to treat the problem non-perturbatively, in particular at exceedingly small electrode distances as indicated by figure 2 and demonstrated by Lang [44].

The main difficulty is evaluating the M_{ts} tunnelling matrix elements (TMEs). Bardeen showed [30] that the tunnelling matrix elements can be expressed as an integral over a surface S lying between the tip and sample in the region where the V_{t} and V_{s} potentials of both electrodes are negligibly small:

$$M_{\mathrm{ts}} = \int \mathrm{d}\vec{S}\vec{\mu}_{\mathrm{ts}}\left(\eta, \xi\right) \tag{10}$$

where η, ξ are the inner coordinates of the surface. The expression for $\vec{\mu}_{ts}(\eta, \xi)$, the position-dependent overlap of the wavefunctions of the electrodes, is formally similar to the expression of quantum mechanical current density:

$$\vec{\mu}_{ts} = \left(\psi_t^* \vec{\nabla} \psi_s - \psi_s^* \vec{\nabla} \psi_t\right). \tag{11}$$

3.1. The tube–substrate tunnel junction

One of the significant differences between the STM measurements of the surfaces of bulk materials and those on supported carbon nanotubes is the existence of a second tunnelling gap [28, 29] in the latter case. This second tunnelling gap is that between the CNT and its support, because the nanotube floats at a distance 0.335 nm over the support surface due to van der Waals interactions. Since in order to measure a tunnelling current the electron has to pass through both tunnel gaps, the STM image is determined by the characteristics of both tunnel junctions. In order to separate the effects of the different junctions it is interesting to compare their transmittivity. Hence we calculated, using the Bardeen formalism, the tunnelling matrix element (TME) between the $m = 0$ state of the tube (see section 2) and the corresponding state of the substrate where, the substrate wavefunction is an eigenstate of a semi-infinite 3D jellium potential with a plane surface using the same potential parameters as in the case of the CNT. The $M_{tube-substrate}$ matrix element is a function of tube length; hence in order to be consistent with the WPD simulations we considered the axial length of the axial charge spreading of electrons during the tunnelling, corresponding to a length section of about 5 nm calculated using the same potential parameters and geometry [29]. Then, for the sake of comparison, we also calculated the tunnelling matrix element, $M_{tip-tube}$, between the $m = 0$ eigenstate of the tube, and an s-wave type eigenstate of a spherical tip with 0.5 nm radius of curvature, at a distance 0.409 nm above the tube. In the region of interest for tunnelling, the tip wavefunction has an asymptotic spherical form, similar to the one used by Tersoff and Hamann [45] in their description of STM measurements of bulk surfaces. When considering the ratio of these two TMEs for the particular configuration used in our WPD simulations, we found $M_{tip-tube}/M_{tube-substrate} = 2.34 \times 10^{-3}$. Since the tunnelling probability (current) is proportional to the square of the corresponding matrix elements, the tunnel resistance of the tip–CNT junction turns out to be much larger than the tube–substrate tunnel resistance, for tip–tube distances away from the point contact regime. The larger tunnelling resistance determines the tunnelling current and hence the characteristics of the STM images of carbon nanotubes.

Therefore we conclude that the second tunnelling gap—that between the nanotube and the substrate—does not significantly affect the measured tunnelling current; hence it cannot be responsible for discrepancies in the apparent height of the nanotubes observed in STM measurements for conductive substrates. However, the presence of a thin oxide layer or other contaminations may seriously affect these results.

The above justified findings were successfully applied as an assumption in the tight binding theory for calculation of atomic resolution STM images of carbon nanotubes [46].

3.2. The tip–tube and tip–substrate tunnel junction

Although theories considering the STM tip as a mathematical point source of current have been successfully applied in many cases [45], the effects arising from the finite extent and geometry of the STM tip are well known (e.g. the tip–sample convolution effects). These effects have been studied experimentally and successfully described theoretically using the WPD method [28].

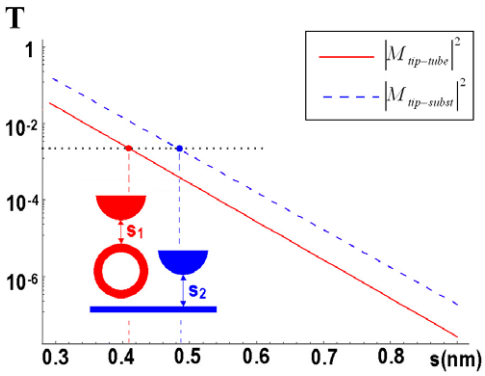

Figure 5. Transmission probabilities for the STM tip–CNT (full line) and STM tip–substrate (dashed line) systems as a function of tunnel gap s, showing an exponential-like decay of the tunnelling probability. Note that not only are the lines shifted relative to each other, but their slopes are also slightly different. The inset shows the mechanism for the flattening of the tube (see the text for details).

Although not affected by tip convolution effects, discrepancies in the apparent height of the nanotubes measured by STM also occur [14–16]. Measuring the height of the nanotubes practically means comparing tunnelling currents for the STM tip positioned over the top of the tube with that above the substrate, which means comparing tunnel currents flowing through the tip–CNT and tip–support tunnel junctions, respectively.

In order to study this problem, we have calculated the TMEs of the tip–CNT (and tip–substrate) junctions as a function of tip–CNT (tip–substrate) distances. The results are shown in figure 5.

Our results show an exponential-like decay of tunnelling probability with distance, and also reproduce the one order of magnitude decay on every ångström distance, a rule of thumb derived from experimental observations.

In the most common, constant current operating mode, the STM tip follows a constant electronic density of states (DOS) surface weighted by the tunnelling probability. Since the difference in the DOS of the CNT and the support seems to affect little the apparent height of the nanotubes [7], it is more relevant to compare the tunnelling probabilities above the CNT and substrate. According to figure 5, in order to maintain a constant tunnelling probability $M_{\mathrm{tip-tube}}(s_1) = M_{\mathrm{tip-plane}}(s_2)$ above the CNT and substrate the STM feedback loop has to retract the tip from the value $s_1 = 0.409$ nm above the CNT to the value $s_2 = 0.485$ nm above the substrate; hence an apparent flattening of about 10% of the tube occurs.

We found that there are two main reasons responsible for the apparent flattening of the nanotubes in STM measurements (according to the above discussed: no mechanical deformation of the tube or difference in the electronic structure relative to the substrate is present).

The first reason can be illustrated by plotting the Bardeen matrix element densities $\mu_{\mathrm{tip-tube}}(x, y)$ on a plane surface inside the vacuum barrier between the STM tip and the CNT (respectively the STM tip and the substrate $\mu_{\mathrm{tip-substrate}}(x, y)$). As was noted above, this quantity measures the local overlap of the unperturbed wavefunctions of the electrodes inside the tunnel gap.

As can be seen in figure 6, the shape of the tunnelling channel of the STM tip–CNT junction is asymmetric, (i.e. wider along the tube axis than along the circumference), because the tunnelling channel narrows in the circumferential direction, due to the shape of the CNT's wavefunctions, which in turn are primarily determined by the curvature of the tube.

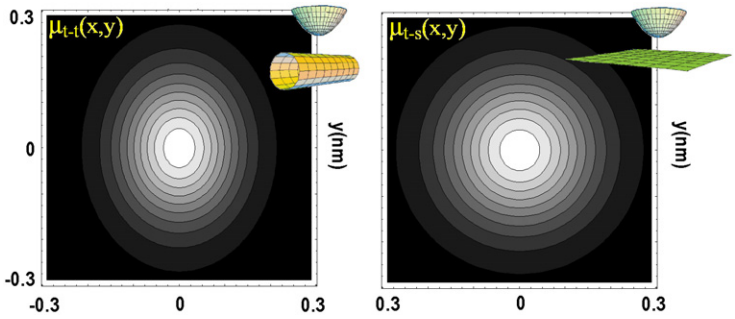

Figure 6. Cross sectional plot of the tip–tube (left) and tip–substrate (right) tunnelling channel represented by the tip–tube (tip–substrate) tunnelling matrix element density on a plane inside the vacuum gap between the STM tip and nanotube (substrate) for a 0.409 nm tunnel gap in both cases. The grey scales are identical in both figures.

The transmission probability can be obtained by integrating the $\mu(x, y)$ functions on the (x, y) plane. It is easy to anticipate from figure 6 that in the case of the tip–tube tunnel junction this value will be smaller than in case of the tip–substrate tunnel junction, due to the shrinking of the tunnelling channel along the circumference of the tube. This effect is even more accentuated for smaller tube diameters.

The second reason for the flattening observed in our model is related to the connection between the decay rate of tunnelling probabilities and the complex 3D geometry of the tunnelling gap.

The distance dependence of the tunnelling probability is usually written as

$$T \propto \mathrm{e}^{-2\chi s}, \qquad \text{where } \chi = \sqrt{2(V_0 - E)} \tag{12}$$

gives the decay rate of the tunnelling probability with distance. This behaviour is quite general as it is derived from various models of tunnelling through one-dimensional barriers [47].

From figure 5 it is obvious that both the tip–tube and tip–substrate tunnelling junctions show an exponential-like decay. However, when we calculate the decay rate of the fitted exponentials we find $\chi_{\mathrm{tip-tube}} = 11.62\ \mathrm{nm}^{-1}$ for the tip–tube tunnel junction, and $\chi_{\mathrm{tip-substrate}} = 11.34\ \mathrm{nm}^{-1}$ for the tip–support tunnel junction, which are slightly different from χ calculated using the 1D tunnelling theory, where $\chi = \sqrt{2(V_0 - E)} = 11.24\ \mathrm{nm}^{-1}$ corresponding to two planar electrodes in 3D. In order to clarify the effect of the curved 3D geometry, we calculated the effective decay rate χ for a blunt tip and a large-diameter tube in order to approach the plane–plane tunnel junction situation. The χ decay rate in this case was found to be $\chi = 11.24\ \mathrm{nm}^{-1}$, practically equal to the one predicted by 1D tunnelling theory (two planar electrodes). Hence we attribute the differences found in the effective decay rate to the curvature of the electrodes (in the case of $\chi_{\mathrm{tip-tube}}$ due to the curvature of both tip and nanotube, while in the case of $\chi_{\mathrm{tip-substrate}}$ due only to the curvature of the tip). Therefore this effect is closely related to the 3D tunnel barrier geometry.

The main conclusion of this result is that the decay rate of the tunnelling probability increases with increasing curvature of the electrodes. Therefore the difference in the decay rates of the 'tip–tube' and 'tip–substrate' tunnel junctions also contributes to the apparent flattening of the nanotubes in STM measurements. This effect is responsible for the difference in the slopes of the lines in figure 5, which gives rise to a tip–sample distance-dependent flattening of the tubes.

Our findings related to the increased effective decay rates attributed to the geometry of the tunnel junction are in good agreement with the results of Garcia *et al* [48], who used a scattering

approach for the description of tunnelling between a periodic array of tips and a jellium surface. They found that the tip curvature increases the decay rate of the tunnelling probability, and included this increase in the exponential factor 2 of equation (12), which became 2.14 for an atomically sharp tip.

Both of the effects mentioned above leading to the apparent flattening of the tube in STM measurements increase with decreasing tube diameter, which is in agreement with the experimental findings of Olk and Heremans [49], who found an increasing deviation with decreasing tube diameter for the diameter measured by STM and that calculated from spectroscopic data.

4. Conclusions

We studied within the framework of a simple model system the geometrical effects influencing the tunnelling probabilities in STM configurations, which are proposed to be the main factors responsible for discrepancies between the apparent height of the nanotubes measured by STM and their real diameter. We propose two main factors influencing the image formation mechanism: (1) the shrinkage of the tunnelling channel in the circumferential direction, due to the curvature of the tube, and (2) the increased decay rate of tunnelling probabilities for curved electrodes (as compared to planar ones). A faster decay with smaller curvature radii was found. For a tube with 1 nm diameter a flattening of about 10% is predicted by the calculated geometry-related effects. These effects are also dependent on the CNT's diameter and the tip–sample distance. An increasing flattening of the tubes is found with decreasing tube diameter and increasing tip–sample distance. Anomalously small diameters can be observed at exceedingly large tip–CNT distances.

Acknowledgments

This work has been partly funded by OTKA Grant No T 043685 in Hungary and partly by the IUAP program P5/01 'Quantum size effects in nanostructured materials' of the Belgian Science Policy Programming.

References

[1] Reich S, Thomsen Ch and Maultzsch J 2002 *Carbon Nanotubes: Basic Concepts and Physical Properties* (Berlin: Wiley)
[2] Seidel R, Graham A P, Unger E, Duesberg G S, Liebau M, Steinhoegl W, Kreupl F, Hoenlein W and Pompe W 2004 *Nano Lett.* **4** 831
[3] Bachtold A, Hadley P, Nakanishi T and Dekker C 2001 *Science* **294** 1317
[4] Dresselhaus M S, Dresselhaus G and Eklund P C 1996 *Science of Fullerenes and Carbon Nanostructures* (San Diego, CA: Academic)
[5] Hamada N, Sawada S and Oshiyama A 1992 *Phys. Rev. Lett.* **68** 1579
[6] Mintmire J W, Dunlap B I and White C T 1992 *Phys. Rev. Lett.* **68** 631
[7] Rubio A, Sánchez-Portal D, Artacho E, Ordejón P and Soler J M 1999 *Phys. Rev. Lett.* **82** 3520
[8] Wildoer J W G, Venema L C, Rinzler A G, Smalley R E and Dekker C 1998 *Nature* **391** 59
[9] Odom T W, Huang J L, Kim Ph and Lieber C M 1998 *Nature* **391** 62
[10] Biró L P and Lambin Ph 2003 Scanning tunneling microscopy of carbon nanotubes *Encyclopedia of Nanoscience and Nanotechnology* ed H S Nalwa (Fairfield, NJ: American Scientific Publishers)
[11] Briggs G A D and Fisher A J 1999 *Surf. Sci. Rep.* **33** 1
[12] Biró L P, Gyulai J, Lambin Ph, Nagy J B, Lazarescu S, Márk G I, Fonseca A, Surján P R, Szekeres Zs, Thiry P A and Lucas A A 1998 *Carbon* **36** 689
[13] Meunier V and Lambin P 1998 *Phys. Rev. Lett.* **81** 5588

[14] Venema L C, Meunier V, Lambin Ph and Dekker C 2000 *Phys. Rev.* B **61** 2991
[15] Kim Ph, Odom T W, Huang J L and Lieber C M 2000 *Carbon* **38** 1741
[16] Klusek Z, Datta S, Byszewski P, Kowalczyk P and Kozlowsk W 2002 *Surf. Sci.* **507** 577
[17] Hertel T, Walkup R and Avouris Ph 1998 *Phys. Rev.* B **58** 13 870
[18] Hofer W A, Foster A S and Shluger A L 2003 *Rev. Mod. Phys.* **75** 1287
[19] Kresse G and Hafner J 1993 *Phys. Rev.* B **47** 558
[20] Kresse G and Furthmuller J 1996 *Phys. Rev.* B **54** 11169
[21] Tersoff J 1986 *Phys. Rev. Lett.* **57** 440
[22] Ogando E, Torsti T, Zabala N and Puska M J 2003 *Phys. Rev.* B **67** 075417
[23] Ogando E, Zabala N and Puska M 2002 *Nanotechnology* **13** 363
[24] Yannouleas C, Bogachek E and Landman U 1998 *Phys. Rev.* B **57** 4872
[25] Venema L C, Widoer J W G, Janssen J W, Tans S J, Temminck H L J, Louwenhoven L P and Dekker C 1999 *Science* **283** 52
[26] Wu J, Duan W, Gu B L, Yu J Z and Kawazoe Y 2000 *Appl. Phys. Lett.* **77** 2554
[27] Márk G I, Biró L P and Gyulai J 1998 *Phys. Rev.* B **58** 12645
[28] Márk G I, Biró L P, Gyulai J, Thiry P A, Lucas A A and Lambin P 2000 *Phys. Rev.* B **62** 2797
[29] Márk G I, Biró L P and Lambin P 2004 *Phys. Rev.* B **70** 115423
[30] Bardeen J 1961 *Phys. Rev. Lett.* **6** 57
[31] Tersoff J 1989 *Scanning Tunneling Microscopy and Related Methods* (*NATO ASI Series* vol E184) ed R J Behm, N Garcia and H Rohrer, (Dordrecht: Kluwer Academic Publishers) pp 77–95
[32] Orosz L and Balázs E 1986 *Surf. Sci.* **177** 444
[33] Kurti J, Zolyomi V, Kertesz M, Sun G, Baughman R H and Kuzmany H 2004 *Carbon* **42** 971
[34] Tapasztó L, Márk G I, Gyulai J, Lambin P and Biró L P, 2003 *Electronic Properties of Novel Materials-Nanostructures* (*AIP Conf. Proc.* vol 685) ed H Kuzmany, J Fink, M Mehring and S Roth (Melville, NY: American Institute of Physics) p 439
[35] Bowman F 1958 *Introduction to Bessel Functions* (New York: Dover)
[36] Jhi S H, Louie S G and Cohen M L 2000 *Phys. Rev. Lett.* **85** 1710
[37] Pan H, Feng Y P and Lin J Y 2004 *Phys. Rev.* B **70** 245425
[38] Shan B and Cho K 2004 *Phys. Rev.* B **70** 233405
[39] Biró L P, Lazarescu S, Lambin Ph, Thiry P A, Fonseca A, Nagy J B and Lucas A A 1997 *Phys. Rev.* B **56** 12490
[40] Biró L P, Márk G I and Balázs E 1994 *Nanophase Materials* (*NATO ASI Ser.* vol E260) (Dordrecht: Kluwer Academic Publishers) p 205
[41] Mizes H A, Park S and Harrison W A 1987 *Phys. Rev.* B **36** 4491
[42] Ciraci S and Batra I P 1987 *Phys. Rev.* B **36** R6194
[43] Tekman E and Ciraci S 1989 *Phys. Rev.* B **40** 10286
[44] Lang N D 1988 *Phys. Rev.* B **37** R10395
[45] Tersoff J and Hamann D R 1985 *Phys. Rev.* B **31** 805
[46] Meunier V, Senet P and Lambin Ph 1999 *Phys. Rev.* B **60** 7792
[47] Wiesendanger R 1994 *Scanning Probe Microscopy and Spectroscopy* (Cambridge: Cambridge University Press)
[48] Garcia N, Ocal C and Flores F 1983 *Phys. Rev. Lett.* **50** 2002
[49] Olk Ch H and Heremans J P 1994 *J. Mater. Res.* **9** 259